ACS OMEGA

http://pubs.acs.org/journal/acsodf

Article

Statistical Study of the Influence of Electrosynthesis Conditions on the Capacitance of Polypyrrole

Andrés F. Pérez-Torres, Martín González-Hernández, Pablo Ortiz, and María T. Cortés*

Cite This: *ACS Omega* 2022, 7, 15580−15595

Read Online

ACCESS | Metrics & More | Article Recommendations | Supporting Information

ABSTRACT: Polypyrrole (PPy) is a promising material for the fabrication of flexible energy storage devices and much research has been published. However, no statistical tools have been used to relate PPy synthesis conditions to its energy storage performance, considering not only the main synthesis factors but also their interactions. In this work, we use a factorial design of experiments to evaluate the influence of two electropolymerization methods and three synthesis parameters on the energy storage capacity of PPy coatings. The polymers were characterized by cyclic voltammetry (CV), galvanostatic charge/discharge (GCD), electrochemical impedance spectroscopy (EIS), Raman spectroscopy, and scanning electron microscopy (SEM). Statistical tests showed that ClO_4^--doped PPy exhibits higher capacitances than *p*-toluenesulfonate (pTS)-doped PPy, with a maximum capacitance of 353.75 ± 1.6 F g^{-1} at 1 A g^{-1}. However, the pTS-doped PPy had better cycling stability, losing only 10% of its original energy storage capability after 5000 charge−discharge cycles at 1 A g^{-1}. The best energy densities and power densities were 49.1 ± 0.2 Wh kg^{-1} and 2297 ± 15 W kg^{-1} (ClO_4^--doped PPy) and 47.8 ± 1.5 Wh kg^{-1} and 2191 ± 91 W kg^{-1} (pTS-doped PPy), respectively, which indicates that through statistical tools, the optimal synthesis conditions are refined to take advantage of the energy storage properties of this polymer.

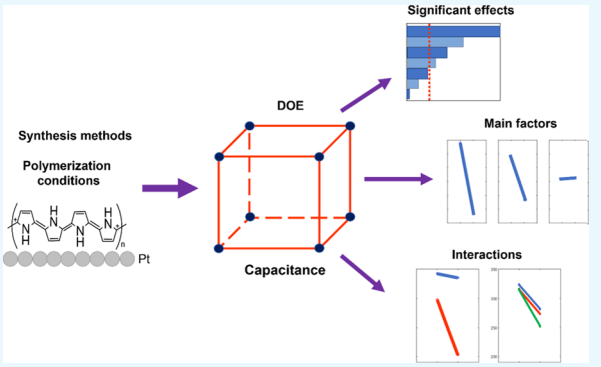

1. INTRODUCTION

The depletion of fossil fuels and the environmental damage resulting from their excessive use have sparked interest in the use of renewable energy sources.[1−5] However, a major constraint to their massive use is the intermittency of energy due to its dependence on weather conditions.[3,6] This makes it imperative to develop and optimize energy storage devices that allow better utilization of the resource generated. In particular, to store all of the energy produced by intermittent energy sources, devices with high power and energy densities are needed.

Energy storage devices include batteries, fuel cells, and capacitors. The first two are characterized by high energy densities (to able to store a lot of energy in a small amount of mass) but require very long charging periods (low power density). Consequently, their use as storage devices for intermittent energy sources is not the most viable since their lifetime is low under these operating conditions and in addition do not collect all of the available energy.[6] On the other hand, capacitors are characterized by high power but low energy density, so they are not useful for storing large amounts of energy.

Supercapacitors are an emerging type of material that aims to fill the technology gap between batteries and capacitors, achieving high energy and power densities. These devices store electrical energy through two different mechanisms, electrostatic double-layer capacitance (EDLC) and fast and reversible surface or near-surface redox reactions[5−7] (pseudocapacitance). The double-layer capacitance is obtained from the energy stored in the Helmholtz double layer especially in large-surface-area electrodes. In the case of pseudocapacitance, the charge (Q) depends on the potential (V) as dQ/dV,[8] and the material behaves to some extent like a battery (faradaic process). However, typical electrochemical responses are quasi-rectangular cyclovoltammograms and quasi-linear galvanostatic charge−discharge (GCD) curves, which resemble those of EDLCs,[8] hence the term "pseudo" in pseudocapacitance. When pseudocapacitive and EDLC mechanisms coexist in the same material, it is referred to as supercapacitive. In all cases, the amount of charge stored is quantified by the specific capacitance (F g^{-1}).

Conjugated conducting polymers (CPs) are among the most promising electrode materials as supercapacitors due to their high charge density, favorable environmental stability, low cost,

Received: January 19, 2022
Accepted: April 5, 2022
Published: April 28, 2022

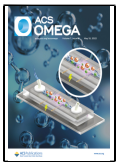

https://doi.org/10.1021/acsomega.1c06843
ACS Omega 2022, 7, 15580−15595

considerable structural diversity, and mechanical flexibility.[4,6,9] The most studied CPs for energy storage and their theoretical specific capacitances are polyaniline (PANi) with 750 F g^{-1}, polythiophene (PTh) with 485 F g^{-1}, polypyrrole (PPy) with 620 F g^{-1}, and ploy(3,4-ethylenedioxythiophene) (PEDOT) with 210 F g^{-1}.[6,10−12] Among the CPs, PPy stands out for its high electrical conductivity, ease of synthesis, and low obtention cost.[9,13,14] The specific capacitances reported for this polymer range from 100 to 650 F g^{-1},[9,11,12,15−18] depending on the synthesis conditions, polymer morphology, dopant nature, and characterization conditions.

There is currently great interest in increasing the energy density and stability of PPy without sacrificing its current power density. To achieve this, it is important to take into account that most of the synthesis parameters significantly influence the physicochemical properties and stability of this polymer. Thus, for example, it is known that the chemical nature of the solvent and the electrolyte affect the microstructure, porosity, conductivity, and cross-linking of PPy. Temperature affects the polymerization kinetics, conductivity, and redox properties.[10] And the type of electrical signal of synthesis causes differences in adhesion, morphology, and homogeneity of the coatings. Even, postsynthesis modifications, such as additional oxidations, lead to changes in the properties of this polymer, such as in its conductivity and electro-constriction. Therefore, it is clearly relevant to perform systematic studies that refine the individual and combined influence of the synthesis parameters on the charge storage properties of PPy. Quite a few studies of how one or two of these parameters affect the electrochemical properties of the polymer are found in the literature; for example, Wang et al. found that the type of dopant ions influenced the capacitance.[19] Raudsepp et al. evaluated the ionic mobility of different sulfonate dopant ions and the electroactivity of the polymer.[20] Oteroet al. observed that the electrodeposition potential, the type of anion, and the total synthesis charge modified the charge storage of the polymer,[21] among others.[21−26] However, there are hardly any publications on the effect of several factors at once, their interactions, and the statistical significance of these parameters on the supercapacitance of PPy. Such an approach holds promise for optimizing synthesis methods and systematically improving the energy storage capacity, thus increasing the chances of obtaining a commercially viable product.

Among the different electrical signals of electropolymerization used with PPy, it has been shown that current pulses and constant current at low current densities favor polymer stability and supercapacitance.[26−29] It is also known that the use of organic solvents during synthesis, such as acetonitrile (ACN), produces polymers with good mechanical and electronic properties; however, water is a widely used solvent because of the high solubilization of pyrrole, salts and because of its environmental advantages.[30] Among the different dopant ions, *p*-toluenesulfonate anions tend to improve the charge/discharge stability of the polymer,[19,24] while ClO_4^--doped polymers generate high capacitances. Postsynthetic modifications of the polymer are uncommon; however, it has been shown that increasing the doping level after synthesis improves the electrochemical properties of PPy as a more active material is obtained.

Therefore, in this work, we study the influence of these synthesis parameters (dopant, solvent, electrical signal, and postsynthetic modification) on the supercapacitance of the electrochemically synthesized PPy. Through statistical analysis, we determine which synthesis parameters and interactions most influence the capacitance of the polymer and conclude which synthesis conditions produce the highest charge storage capacity and stability of the material.

2. EXPERIMENTAL SECTION

2.1. Materials. Pyrrole (99% purity) was distilled prior to use and stored away from light at 3 °C under N_2 atmosphere. All solutions were prepared with type I water with a resistivity of 18.2 MΩ cm unless stated otherwise. Pyrrole (Py) was the monomer used for the fabrication of the polymer, potassium chloride (KCl) was the supporting electrolyte used for electrochemical characterizations, *p*-toluenesulfonic acid (HpTS) and lithium perchlorate ($LiClO_4$) were used as dopants, and acetonitrile (ACN) was used as a solvent for synthesis. These chemicals were purchased from Sigma-Aldrich. Potassium hexacyanoferrate ($K_3[Fe(CN)_6]$) (from Merck) was used as a redox couple for electrochemical impedance spectroscopy (EIS).

2.2. Design of Experiments (DOE) and Synthesis of PPy Coatings. All electrochemical experiments were performed at room temperature in a three-electrode electrochemical cell with a potentiostat PGSTAT302N MetroOhm Autolab, controlled by the software Nova 2.1.5. The potential was measured against a saturated Ag/AgCl reference electrode, the auxiliary electrode was a platinum wire, and the working electrode was a platinum disk with a geometric area of 0.02 cm^2 (BASi) so that with each synthesis PPy coatings were obtained on the disk-shaped platinum surface.

A design of experiments (DOE) was used to set the combination of synthesis parameters that would allow evaluating the influence of the main factors and their interactions (secondary factors) on the supercapacitance of the polymer. The effect of two types of electrical signals during synthesis was evaluated. The first one consisted of a unipolar pulse current of 10 000 pulses, each pulse with an on-time of 10 ms (t_{on}) and a relaxation time of 100 ms (t_{off}). During t_{on}, an oxidative current of 4 mA cm^{-2} was applied to the working electrode. During t_{off}, no current was applied to the electrode. For this synthesis method, named method A, a 2^3 full factorial design was used (Table 1A). The second synthesis method, named method B, consisted of a series of unipolar pulses of current, as in the previous synthesis, but with a current density of 2.5 mA cm^{-2} followed by a period of constant current density of 0.6 mA cm^{-2}. This current was applied for 10 or 25 min. A mixed three-factor general factorial design was used

Table 1. Factors and Levels Used in the Design of Experiments

(A) 2^3 factorial design		
factor	level	
solvent	water	ACN
dopant	ClO_4^-	pTS
post-oxidation current (mA cm^2)	0	1

(B) mixed three-factor general design			
factor	level		
solvent	ClO_4^-	pTS	
constant current (min)	10	25	
number of pulses	100	300	500

https://doi.org/10.1021/acsomega.1c06843
ACS Omega 2022, 7, 15580−15595

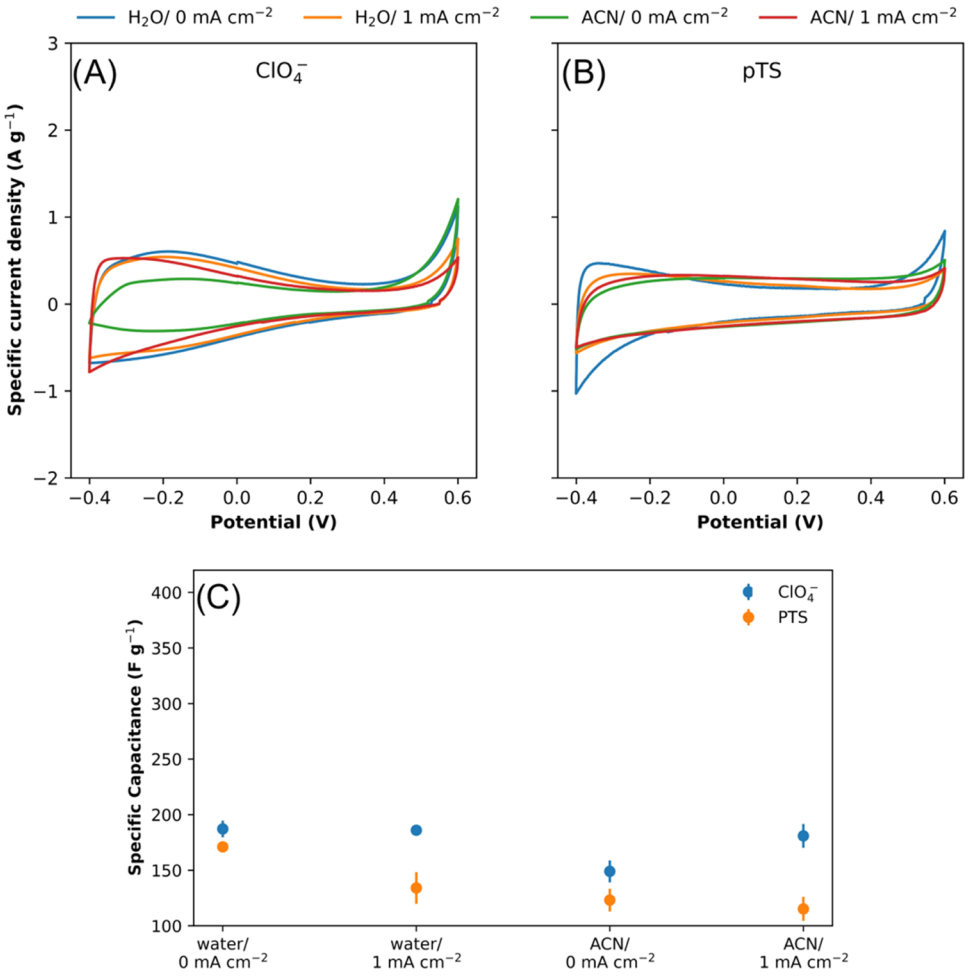

Figure 1. CVs of PPy coatings in 1 M KCl at 5 mV s^{-1}. The polymers were synthesized by method A (10 000 pulses of unipolar current, t_{on} = 10 ms (4 mA cm^{-2}), t_{off} = 100 ms). Blue curve (H_2O/0 mA cm^{-2}) and orange curve (H_2O/1 mA cm^{-2}) represent synthesis without and with post-oxidation of the polymer, respectively (the same applies for ACN). (A) ClO_4^- as dopant. (B) pTS as dopant. (C) Capacitance of PPy coatings determined from CV. The bars correspond to the standard deviation of triplicate measurements.

(Table 1B). The dopant concentration on each synthesis was 0.20 M, and the pyrrole concentration was 0.15 M. All syntheses were carried in water except when ACN (with 2% of water) was one level of the factors to evaluate.

2.3. Characterization. Electrochemical performance of the PPy coatings was investigated by galvanostatic charge/discharge (GCD), cyclic voltammetry (CV), and electrochemical impedance spectroscopy (EIS) techniques. CV measurements were performed in 1.0 M KCl, in a potential window ranging from −0.4 to 0.6 V at a scan rate of 5 mV s^{-1}. For the study of capacitance retention as a function of scan rate, scan velocities ranging from 0.1 to 500 mV s^{-1} were used. Capacitance retention is the percentage of the maximum capacitance that is achieved at different scan rates. The specific capacitance was calculated from CV employing eq 1

$$C_m = \frac{\int I(V)\,dV}{2\,m\,v\Delta V} \tag{1}$$

where C_m (F g^{-1}) is the specific capacitance, I (A) is the current as a function of the potential scan, m (g) is the mass of the polymer, v (V s^{-1}) is the scan rate, and ΔV (V) corresponds to the voltage window.

GCD measurements were performed in 1.0 M KCl, using a potential window ranging from −0.4 to 0.6 V, at a current density of 1 A g^{-1}. The discharge specific capacitance was calculated using the following equation

$$C_m = \frac{I\Delta t}{m\Delta V} \tag{2}$$

where C_m (F g^{-1}) is the specific capacitance, I (A) corresponds to the discharge current, Δt (s) is the discharge time, m (g) is the mass of the polymer, and ΔV (V) is the voltage window. The energy density (Wh kg^{-1}) and power density (W kg^{-1}) were calculated from GCD using eqs 3 and 4, respectively

$$E = \frac{0.5C_m\Delta V^2}{3600} \tag{3}$$

$$P = \frac{E}{\Delta t} \tag{4}$$

where E (Wh kg^{-1}) is the energy density, C_m (F kg^{-1}) is the specific capacitance calculated from GCD, ΔV (V) corresponds to the voltage window, 3600 is used to transform from J or Ws to Wh, P (W kg^{-1}) corresponds to the energy density, and Δt (h) is discharge time from GCD.

EIS experiments were carried out to study the redox processes of the PPy coatings and to evaluate their electronic and ionic conductivities. The Nyquist spectra were taken in 0.5

https://doi.org/10.1021/acsomega.1c06843
ACS Omega 2022, 7, 15580−15595

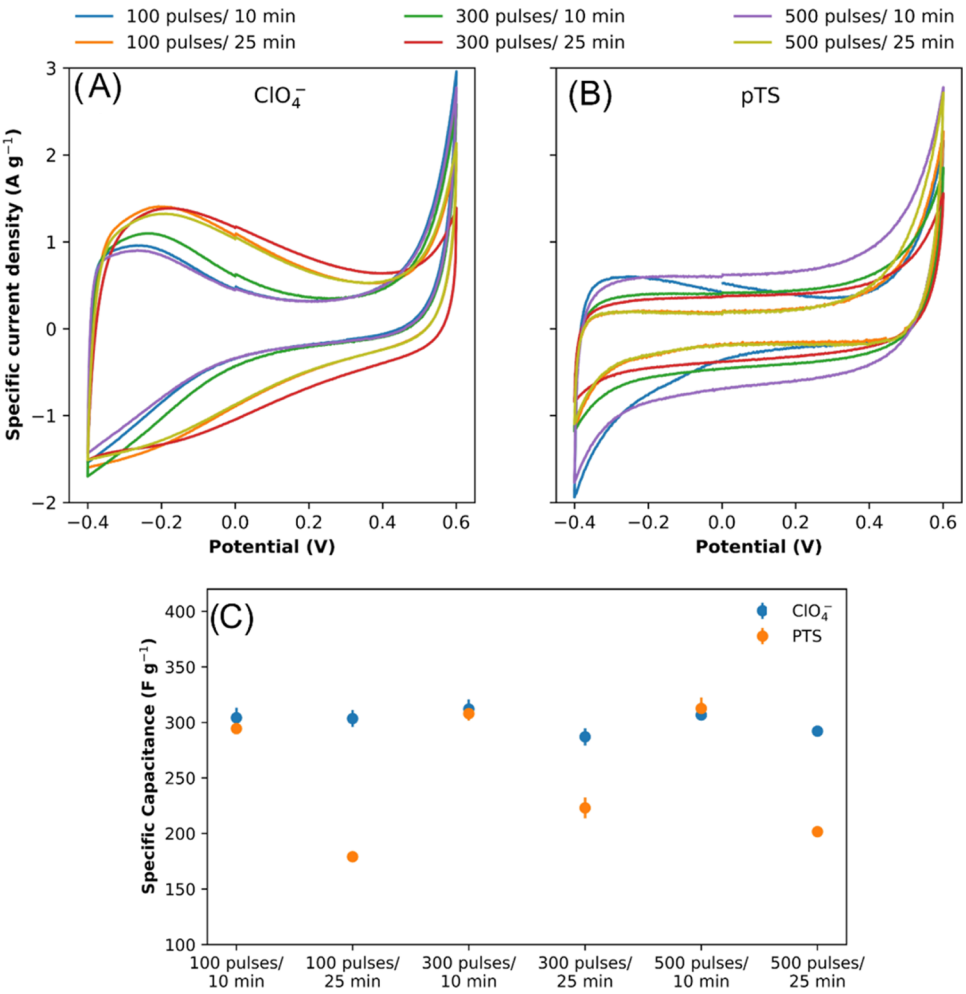

Figure 2. CVs of PPy coatings in 1 M KCl at 5 mV s^{-1}. The polymers were synthesized by method B (pulses of unipolar current, t_{on} = 10 ms (2.5 mA cm^{-2}), (t_{off} = 100 ms) and at the end 0.6 mA cm^{-2} for 10 or 25 min). (A) ClO_4^- as dopant. (B) pTS as dopant. (C) Capacitances of PPy coatings determined by CV. The bars correspond to the standard deviation of triplicate measurements.

M KCl and 5 mM ferricyanide solutions, using an alternating current (AC) amplitude of 10 mV at open-circuit potential, varying frequencies (f) from 100 kHz to 100 Hz. To study the charge storage dynamics of the polymers, measurements were performed from 10 mHz to 10 Hz in 0.5 M KCl and 5 mM ferricyanide solutions using an AC amplitude of 10 mV, varying the potential from −0.4 to 0.6 V with a step of 51.3 mV. The results were used to calculate the real capacitance component (C') as a function of angular frequency ($\omega = 2\pi f$) using the following equation:

$$C' = \frac{-Z''}{\omega |Z(\omega)|^2} \quad (5)$$

The morphology of the coatings was studied by scanning electron microscopy (SEM, JEOL model JSM 6490-LV). Raman spectra were acquired using a 638 nm laser in a range between 1800 and 800 cm^{-1} using an XploRA One Horiba Scientific Instrument.

3. RESULTS AND DISCUSSION

3.1. Supercapacitance from CV and GCD. Cyclic voltammetry (CV) is a widely used characterization technique for conducting polymers. CV allows studying the behavior of the material at different voltages, to calculate the specific capacitance and determine the effect of the scan rate on the capacitive response. In CV analysis, the larger the area under the curve of the cyclovoltammogram, the higher the capacitance of the material. For synthesis method A (Figure 1), ClO_4^--doped polymers showed higher capacitances than those doped with pTS. When using ClO_4^- as a dopant, the polymers with the highest supercapacitance are those synthesized in water without post-oxidation current (187.22 ± 4.73 F g^{-1}) and in ACN with post-oxidation current (180.92 ± 11.47 F g^{-1}). In this case, the difference between the two materials is not statistically significant. For the pTS-doped PPy, the material synthesized in water without post-oxidation current had the highest supercapacitance with 171.06 ± 20.17 F g^{-1}. The ClO_4^--doped polymers show low capacitances when fabricated in ACN or water, with post-oxidation current, being lower when synthesized in ACN without post-oxidation current. In the case of pTS-doped polymers, the capacitance is lower when a post-oxidation current is applied or ACN is used as a solvent. Further analysis of this behavior is shown below with the results of analysis of variance (ANOVA).

For method B (unipolar current pulses as method A but with a current density of 2.5 mA cm^{-2}, followed by a constant current of 0.6 mA cm^{-2} for 10 or 25 min), the most capacitive materials are those synthesized with ClO_4^- using 300 pulses

https://doi.org/10.1021/acsomega.1c06843
ACS Omega 2022, 7, 15580−15595

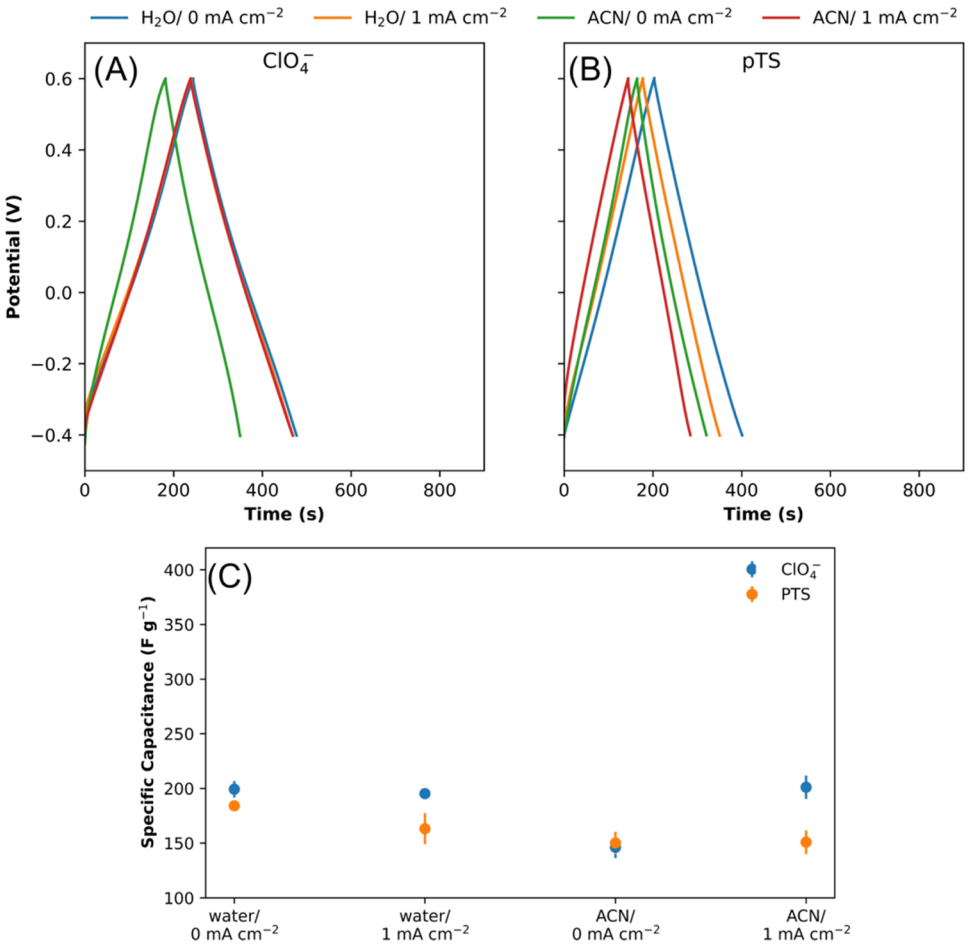

Figure 3. GCD curves of PPy coatings synthesized by method A in 1 M KCl at 1 A g^{-1}. Blue line (H_2O/0 mA cm^{-2}) and orange line (H_2O/1 mA cm^{-2}) represent synthesis without and with post-oxidation of the polymer, respectively (the same applies for ACN). (A) ClO_4^- as dopant. (B) pTS as dopant. (C) Capacitances of PPy coatings determined by GCD. The error bars correspond to the standard deviation of triplicate measurements.

and 10 min of constant current, and those doped with pTS using 500 pulses and 10 min of constant current, with supercapacitances of 313.4 ± 8.5 and 312.6 ± 9.8 F g^{-1}, respectively (Figure 2). The energy storage capacity of the ClO_4^--doped PPy is not statistically different from the pTS-doped polymer when a constant current is applied for 10 min during synthesis. However, when the current is applied for 25 min, the capacitance of the pTS-doped material decreases drastically. Because pTS-doped PPy tends to form compact layered structures, it is likely that ion diffusion decreases as the layer thickness increases.[19] Therefore, the inner part of the polymeric matrix no longer participates in the charge storage process and is possibly overoxidized due to the slow diffusion of anions to stabilize the positive charges formed during the charging process (oxidation). This behavior will be further analyzed with ANOVA results. The almost rectangular shape of the CVs in the pTS-doped polymers, for both synthesis methods, indicates a quasi-ideal capacitive behavior in this potential window.[9] Deviations from this behavior, more significant in the ClO_4^--doped polymers, can be caused by faradaic reactions associated with the oxidation or reduction of the material during the charge/discharge process. These deviations differentiate EDCLs from pseudocapacitors and correspond to anodic or cathodic waves associated with the expulsion or incorporation of ions into the polymer matrix to maintain the electrical neutrality of the system.[31]

GCD was used as a complementary characterization technique to corroborate the results obtained from CV. This technique is more reliable for determining the energy storage capacity of the polymer, as it simulates the charge/discharge process to which energy storage devices are exposed. Also, it provides useful information such as ohmic loss due to internal resistance and allows calculation of the power density and energy density of the material. In the case of the GCD experiments, the longer it takes to discharge the polymer at a constant current density, the higher the capacitance. The results agree with those obtained by CV, presenting the same capacitive trend for the different coatings. The high symmetry between the charge and discharge curves indicates a high reversibility of the process. For method A (Figure 3), the highest capacitances of PPy-ClO_4^- were for the polymers synthesized in water without post-oxidation current (199.3 ± 7.52 F g^{-1}) and for the one synthesized in ACN with post-oxidation current (201.6 ± 10.69 F g^{-1}). For PPy-pTS, the best capacitance was obtained by the synthesis in water without post-oxidation current (184.14 ± 0.51 F g^{-1}).

The same trend observed from the GCD and CV results makes the agreement between both characterization techniques clear. For method B (Figure 4), the most capacitive PPy-ClO_4^- was the one synthesized with 300 pulses and 10 min of constant current (353.75 ± 1.6 F g^{-1}). For PPy-pTS, the best capacitance was achieved by the material synthesized with 500

https://doi.org/10.1021/acsomega.1c06843
ACS Omega 2022, 7, 15580−15595

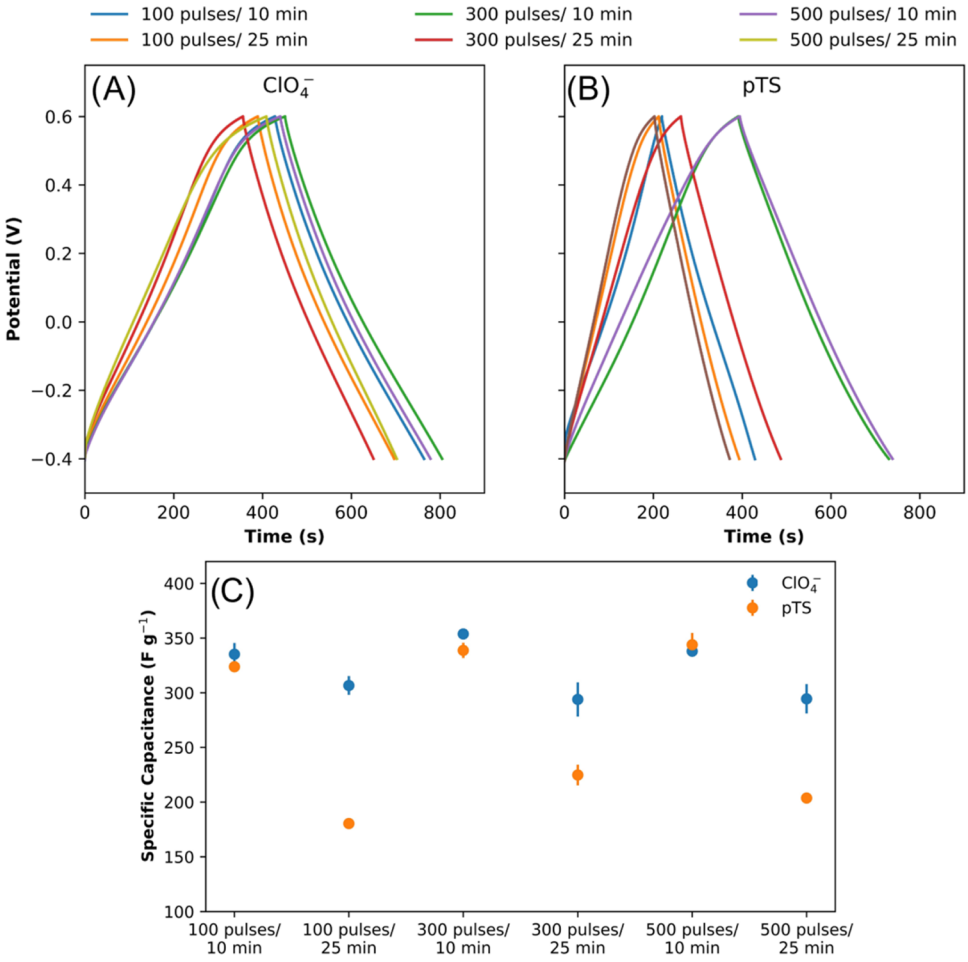

Figure 4. GCD curves of PPy coatings synthesized by method B in 1 M KCl at 1 A g^{-1}. (A) ClO_4^- as dopant. (B) pTS as dopant. (C) Capacitances of PPy coatings determined by GCD. The bars correspond to the standard deviation of triplicate measurements.

pulses and 10 min of constant current (343.88 ± 10.8 F g^{-1}). Again, it is observed that the capacitance of the PPy-pTS obtained by method B is lower when the final constant current is applied for 25 min. The supercapacitances calculated from GCD are slightly higher than those obtained using CV, which is attributed to a slower oxidation/reduction of the polymer at 1 A g^{-1} than at 5 mV s^{-1}. This allows a larger amount of polymer to participate in diffusion-limited ionic insertion or expulsion during the charge/discharge process.

3.2. Further Characterization of Most Capacitive PPy Coatings. The most capacitive polymers for each dopant and synthesis method were chosen for further analysis. Polymers A-H_2O/ClO_4 and A-H_2O/pTS correspond to those obtained by method A, in water, without post-oxidation current, doped with ClO_4^- and pTS, respectively. Polymers B-300,10/ClO_4 and B-500,10/pTS correspond to those obtained by method B, doped with ClO_4^- and pTS, with 300 and 500 pulses, with 10 min of constant current (0.6 mA cm^{-2}) at the end, respectively. The following results correspond to these four polymers.

Electrochemical energy storage is known to be controlled by two different mechanisms: a capacitive process, in which the capacitance is independent of the scan rate, and a semi-infinite diffusion process, which is characterized by a linear behavior with the inverse of the square root of the scan rate.[32] Capacitance retention characterizes the decrease in electrochemical interface area within the structure with increasing scan rates; this is typically due to the limited rate of diffusion of charge-compensating ions at the interface. Higher retention generally suggests better performance, in particular, a higher capacitance obtained even at higher currents and scan rates.[33] In most cases, this decrease in capacitance as a function of the scan rate or charge/discharge current is reported as a % retention with respect to the highest observed value. Figure 5 displays the capacitance retention as a function of scan rate for the selected polymers. Three regions are identified from the plots, the first at high scan rates, where semi-infinite diffusion limits the energy storage process. The second, at intermediate scan rates, corresponds to a transition between an energy storage process limited by semi-infinite diffusion and a purely capacitive process. And the third, at low scan rates, corresponds to a capacitive behavior in which the energy storage is not significantly affected by the scan rate.

As can be seen, the capacitance retention of the polymers obtained by method A is more affected by the scan rate, indicating that these are diffusion-limited more quickly, presenting capacitive behavior only at very low scan rates, below 2 mV s^{-1} for the A-H_2O/ClO_4 polymer and below 0.8 mV s^{-1} for the A-H_2O/pTS polymer. This means that if the polymers are charged or discharged at scan rates above 2 or 0.8 mV s^{-1}, the materials will store 80% or less of the maximum available capacitance. Suggesting that synthesis method A produce dense and compact polymeric structures, which hinders ion diffusion and decrease the active mass of the

https://doi.org/10.1021/acsomega.1c06843
ACS Omega 2022, 7, 15580−15595

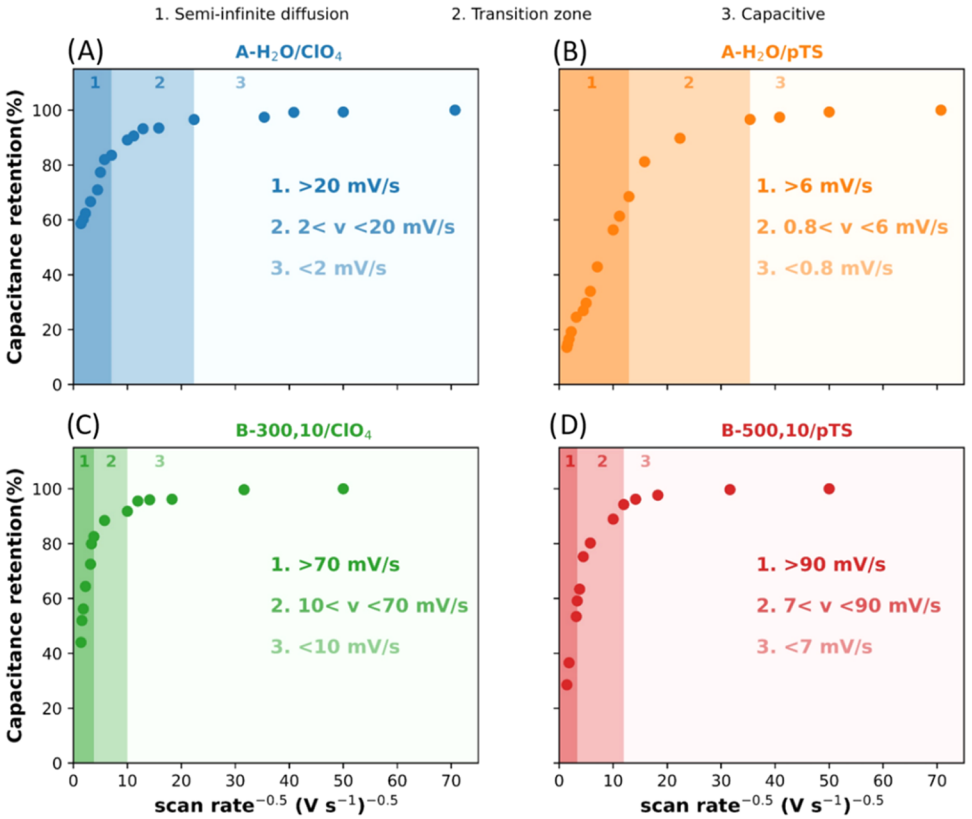

Figure 5. Capacitance retention of PPy coatings as a function of scan rate$^{-0.5}$: (A) A-H_2O/ClO_4, (B) A-H_2O/pTS, (C) B-300,10/ClO_4, and (D) B-500,10/pTS.

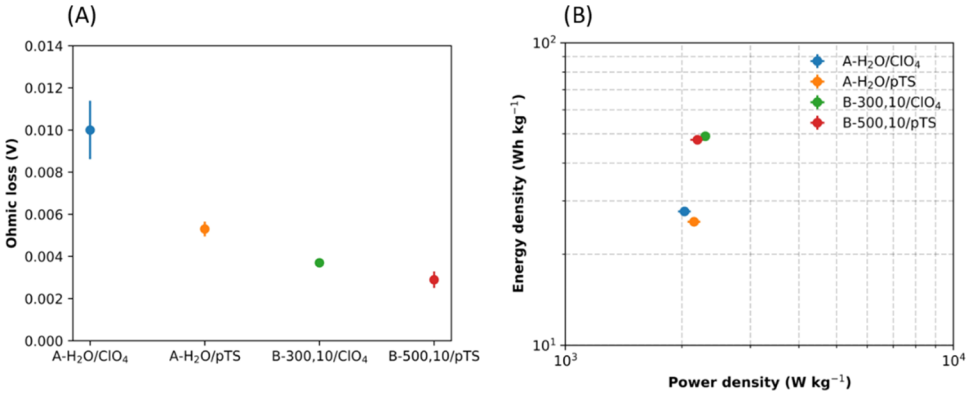

Figure 6. (A) Ohmic loss at 1 A g^{-1} of PPy coatings synthesized under different conditions. The bars correspond to the standard deviation of triplicate measurements. (B) Ragone plot.

polymer involved in the energy storage process.[19] Polymers obtained with method B exhibit a better capacitive behavior, having a complete dependence on diffusion only at scan rates higher than 70 mV s^{-1} for polymer B-300,10/ClO_4 and 90 mV s^{-1} for polymer B-500,10/pTS. This suggests improved ordering of the polymeric matrix, providing more channels for ionic diffusion[26] and improving the capacitance of the polymers obtained by the B method. The lower capacitive performance of the pTS-doped polymers for each synthetic method may allude to the fact that more compact and dense polymeric structures are obtained with this dopant than with ClO_4^-,[19,20,31,34] which hinders the mobility of ions through the material. This is reflected in the drastic decrease in capacitance retention for pTS-doped materials with scan rate, where in the semi-infinite diffusion region there is a loss of 80% or more of the maximum energy storage ability.

The capacitance retention results of the polymers agree with their Ohmic losses (Figure 6A). Here, the lowest Ohmic losses correspond to polymers B-300,10/ClO_4 and B-500,10/pTS, which showed a complete dependence on diffusion only at scan rates higher than 70 and 90 mV s^{-1} (Figure 5). This reinforces the idea that method B generates PPy with more ordered structures that provide channels that favor ionic diffusion and mobility. The Ragone plot (Figure 6B) shows that polymers obtained by synthesis method B have higher energy densities than those obtained by method A, indicating better performance as an energy storage material.

EIS was used to study the redox processes (charge/discharge) and the electronic and ionic conductivities of

https://doi.org/10.1021/acsomega.1c06843
ACS Omega 2022, 7, 15580−15595

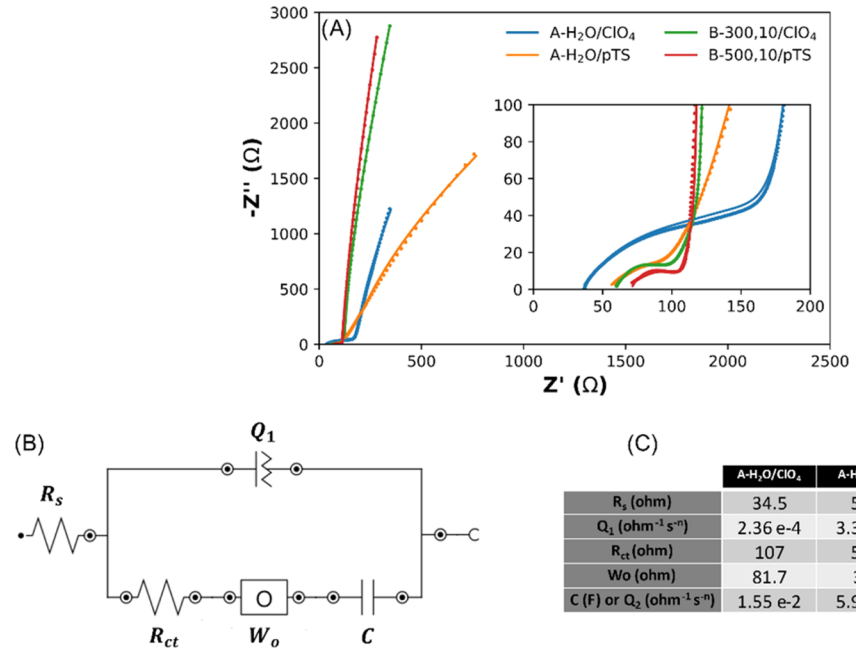

	A-H_2O/ClO_4	A-H_2O/pTS	B-300,10/ClO_4	B-500,10/pTS
R_s (ohm)	34.5	53.6	58.9	70.5
Q_1 ($ohm^{-1} s^{-n}$)	2.36 e-4	3.37 e-4	7.44 e-5	6.03 e-5
R_{ct} (ohm)	107	55.1	43.2	34.9
Wo (ohm)	81.7	387	74.5	44.3
C (F) or Q_2 ($ohm^{-1} s^{-n}$)	1.55 e-2	5.97 e-4	7.02 e-4	6.36 e-4

Figure 7. (A) Nyquist plot of PPy coatings synthesized under different conditions, (B) equivalent circuit, and (C) equivalent circuit parameters.

polymers.[19,27] All spectra were successfully fitted to the equivalent circuit shown in Figure 7B, which is a variation of the Randles circuit. Such a circuit and its modifications have been widely used to interpret EIS results of conducting polymers.[35−38] More complex circuits, for example, using dual-channel transmission lines, have also been employed to further investigate the porosity characteristics of these materials.[24,39−41] The Nyquist impedance plots (Figure 7A) show a semicircle in the high-frequency region, which is associated with charge transfer processes, while its distortion is attributed to material heterogeneity.[42] The linear part in the low-frequency region is governed by the anionic doping/undoping process of PPy.[9,43,44] The diameter of the semicircle corresponds to the interfacial charge transfer resistance between the active material and the electrolyte (R_{ct}), while the intercept of the semicircle on the real axis comprises the solution bulk resistance and the intrinsic resistance of the active material (R_s).[9,28,29,45] From Figure 7C, polymer A-H_2O/ClO_4 has the lowest value of R_s, A-H_2O/pTS and B-300,10/ClO_4 have similar values and B-500,10/pTS has the largest value. This suggests that polymer B-500,10/pTS has the highest resistance of all polymers; however, this is contradictory to the previous results. The cause of this behavior comes from small variations in the distance between the working and reference electrode in the experimental setup, with the value of R_s being proportional to the distance between the electrodes. The constant phase element (Q_1) is associated with the resistance coming from the disordered ionic diffusion at the inhomogeneous electrode/electrolyte interface.[46] The values of Q_1 and R_{ct} indicate that the polymers synthesized with method B have lower resistances than those of method A, indicating higher interfacial charge transfer due to better diffusion of ions into the polymer matrix. These results are in agreement with the Warburg open element (W_0), which describes the resistance caused by finite diffusion of ions within the porous electrode.[47] A higher slope of the line located in the low-frequency region indicates a more capacitive behavior,[28,44] a slope of 90° characterizes an ideal capacitive behavior and a slope of 45° to a process under ionic diffusion control.[13,25,45] As can be seen, the polymers synthesized by method A present processes under diffusion control while the polymers obtained by method B are closer to ideal capacitive behavior. The last element of the model, C or Q_2 in the case of polymer A-H_2O/ClO_4, is proportional to the double-layer capacitance, which is associated to the surface area. This suggests that polymer A-H_2O/ClO_4 has the largest surface area of all polymers.

To study the charge storage dynamics of the selected supercapacitors, EIS measurements were performed between 10 mHz and 10 Hz (Figures 8 and S1−S4). At these frequencies, the electrodes manifest predominantly a capacitive response[48,49] with a distinctive behavior depending on the energy storage mechanism, which can be evaluated through C' and ϕ. The phase angle (ϕ) provides information of the rate-limiting kinetics, acquiring a value of $\phi = 90°$ for a purely capacitive response, $\phi = 45°$ for a diffusion-limited response, and $\phi = 0°$ for a pure resistor.[49] In the case of an EDLC, both C' and ϕ remain nearly constant throughout the voltage window at any given frequency.[48,49] In the case of pseudocapacitors, energy storage is both frequency- and potential-dependent, and is characterized by relatively high values of C', where there are diffusion limitations (indicated by low values of ϕ).[49] From Figure 8, it is observed that polypyrrole electrodes present complex charge storage dynamics, exhibiting a combination of double-layer and pseudocapacitive mechanisms at the same time. At high frequencies (10−1 Hz), there is little or no energy storage, mainly due to diffusion limitations. As the frequency decreases, the contribution of the double-layer and pseudocapacitance in energy storage increases. In the case of a pure EDLC, C' and ϕ would have maximum values at the lowest frequency and decrease slightly at higher frequencies, having almost the same values at every potential for each frequency.[49] In this case, the curvatures of both C' and ϕ suggest the superposition of the pseudocapacitive behavior with that of the double-layer behavior, a consequence of the intricate relationship between potential, diffusion, and energy storage.

https://doi.org/10.1021/acsomega.1c06843
ACS Omega 2022, 7, 15580−15595

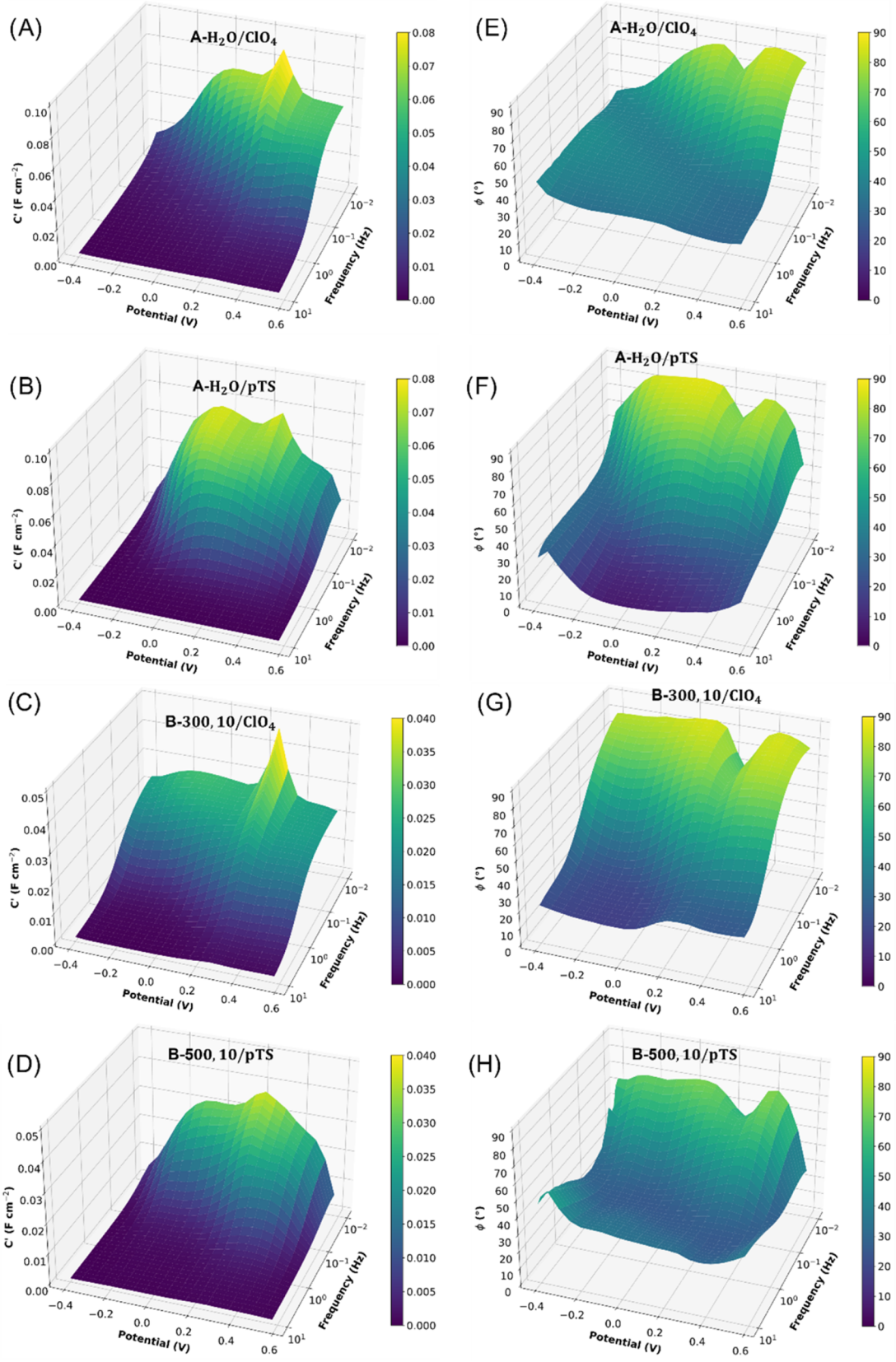

Figure 8. Three-dimensional (3D) Bode plot of area-normalized capacitance (C') vs potential vs frequency (A–D) and phase angle (ϕ) vs potential vs frequency (E–H) for (A, E) A-H_2O/ClO_4, (B, F) A-H_2O/pTS, (C, G) B-300,10/ClO_4, and (D, H) B-500,10/pTS.

The chemical structure of the polymers was investigated by Raman spectroscopy (Figure 9). The broad shape of the peaks suggests that they are amorphous solids with short conjugation lengths.[50] The peaks around ~920 and ~960 cm^{-1} are assigned to deformations of the aromatic ring by the presence of bipolarons and polarons, respectively.[51−55] Peaks around

https://doi.org/10.1021/acsomega.1c06843
ACS Omega 2022, 7, 15580−15595

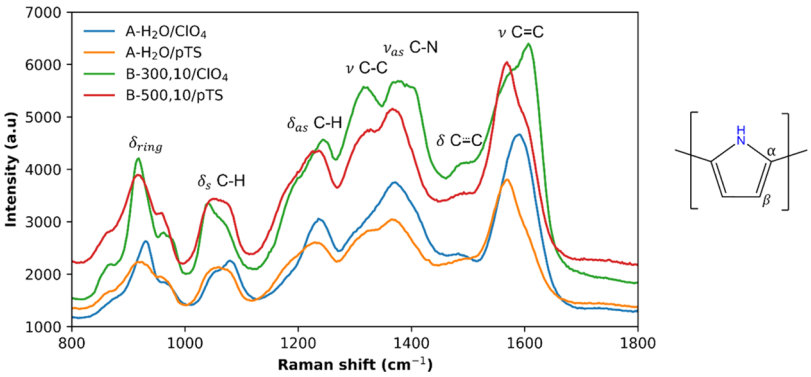

Figure 9. Raman spectra of PPy coatings synthesized under different conditions.

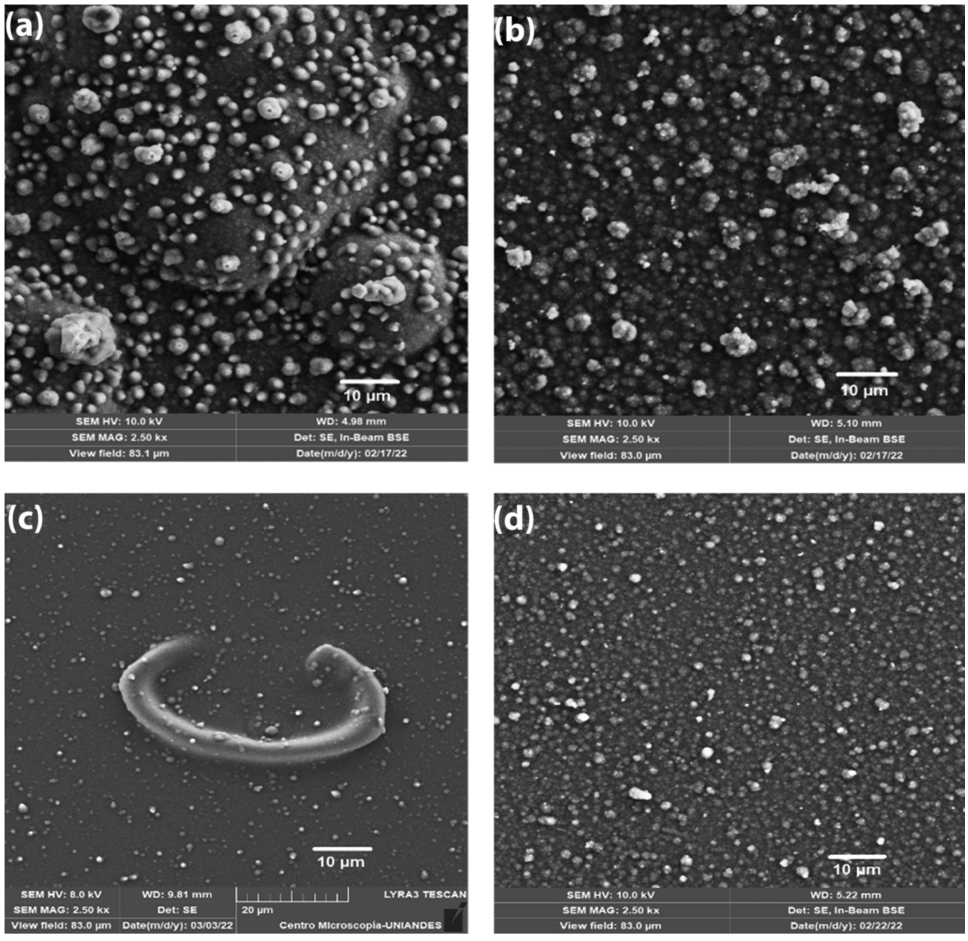

Figure 10. SEM images of (a) A-H_2O/ClO_4, (b) A-H_2O/pTS, (c) B-300,10/ClO_4, and (d) B-500,10/pTS.

~1050 and 1077 cm^{-1} correspond to the symmetric C−H in-plane bending vibrations of the polaron and bipolaron states, respectively.[51,54] The peak at ~1237 cm^{-1} comes from the antisymmetric C−H in-plane bending.[51,52,55] The peak at ~1322 cm^{-1} corresponds to the C−C inter-ring vibration.[54,56] The peak at ~1370 cm^{-1} corresponds to antisymmetric C−N stretching.[13,51] The peak at ~1485 cm^{-1} is assigned to PPy skeletal band.[50,52,54] The peaks at ~1571 and 1600 cm^{-1} arise from the C═C stretching of the polaron and bipolaron states, respectively.[55,56] The presence of antisymmetric C−H bending of the β hydrogens around 1237 cm^{-1} indicates that the pyrrole rings are linked mainly by $\alpha-\alpha'$ bonds, so the polymers have a few branches and therefore high quality.[57] The ratio of peak intensity at ~960 and ~920 cm^{-1} (bipolarons and polarons, respectively) was higher for ClO_4^--doped polymers, with values of 1.50 for B-300,10/ClO_4, 1.42 for A-H_2O/ClO_4, 1.22 for B-500,10/pTS, and 1.14 for A-H_2O/pTS. This depicts a higher level of doping[50] and hence higher capacitance for ClO_4^--doped polymers than for pTS-doped polymers.

SEM images show that A-H_2O/pTS and B-500,10/pTS polymers have a similar structure with different particle diameters, while A-H_2O/ClO_4 and B-300,10/ClO_4 polymers have different morphologies (Figure 10). Polymer A-H_2O/ClO_4 has an average floret diameter of 17.3 μm and an average particle diameter of 1.1 μm. A-H_2O/pTS has a homogeneous distribution of spherical particles with an average particle

https://doi.org/10.1021/acsomega.1c06843
ACS Omega 2022, 7, 15580−15595

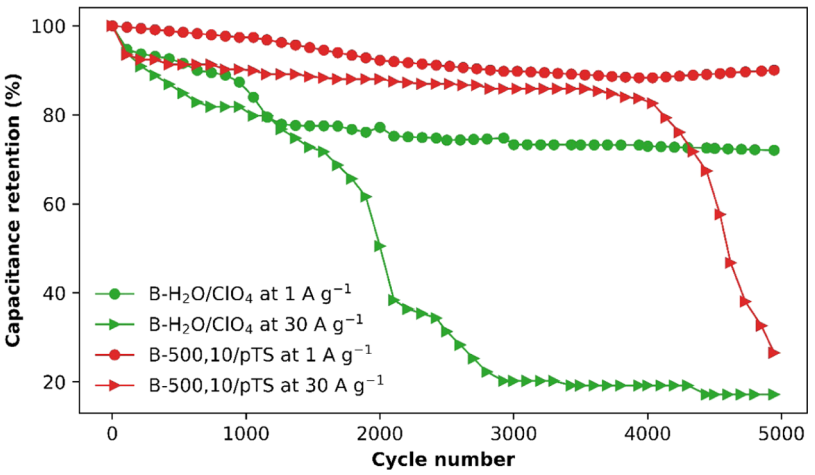

Figure 11. Stability study of PPy coatings synthesized under different conditions.

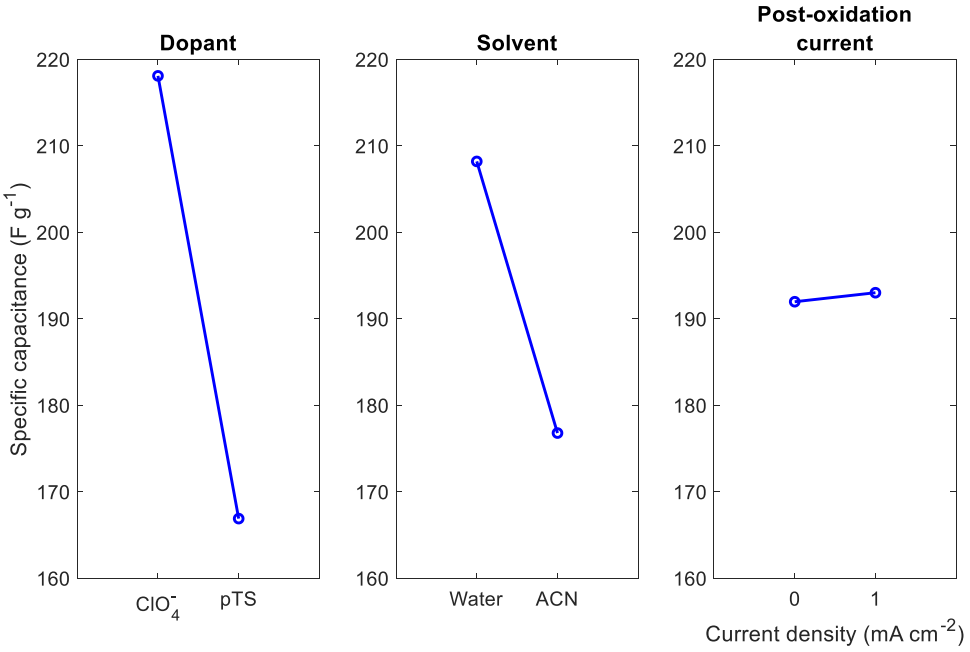

Figure 12. Main effects plot for synthetic method A.

diameter of 0.9 μm. B-300,10/ClO_4 shows the presence of C-shaped structures along with spherical particles covering the whole surface. The spherical particles have a mean diameter of 0.5 μm, while the C-shaped structures have an average 2D projected area of 242.2 μm^2. B-500,10/pTS consists of spherical particles with an average diameter of 0.3 μm. Figure S8 shows histograms with the particle size distribution of the different polymers. Homogeneous small spherical structures such as those of polymers obtained by method B are expected to ease charge transfer processes and improve polymer's supercapacitance.[28] In general, it is well known that the morphology of these polymers is decisive for their charge storage properties. For example, Wei et al., Wang et al., and Aiping et al. showed that the morphology of PPy coatings influences the ionic transport through the polymer by defining the uniformity and stability of the channels and thus contributes to their capacitance. This has been observed especially from electrochemical characterizations and SEM images.[19,52,58]

Stability studies were performed for the B-300,10/ClO_4 and B-500,10/pTS polymers, as these showed the best supercapacitive performance (Figure 11). B-300,10/ClO_4 showed low cycling stability, losing about 30% of its capacitance (at 1 A g^{-1}) and about 80% (at 30 A g^{-1}), for 5000 cycles. B-500,10/pTS showed greater stability, losing only about 10% of its energy storage capacity at 1 A g^{-1} or in 4000 cycles at 30 A g^{-1}. Polymer degradation commonly originates from electrical and electrochemical damage to the material.[41] Overoxidation causes the polymer chains to form C−O bonds and/or cross-linking between chains;[24,41] in addition, morphological changes in the polymer matrix result in loss of conductivity.[41] Morphological alterations arise from the volumetric changes of the polymer caused by its swelling and shrinking due to the insertion and ejection of anions during the charge/discharge. Because pTS is a considerably larger anion than ClO_4^- and, in addition, when used as a dopant, it produces more compact polymers; during the charge/discharge process, there is less expulsion of pTS and, therefore, less volumetric changes of the polymer, leading to greater stability.

https://doi.org/10.1021/acsomega.1c06843
ACS Omega 2022, 7, 15580−15595

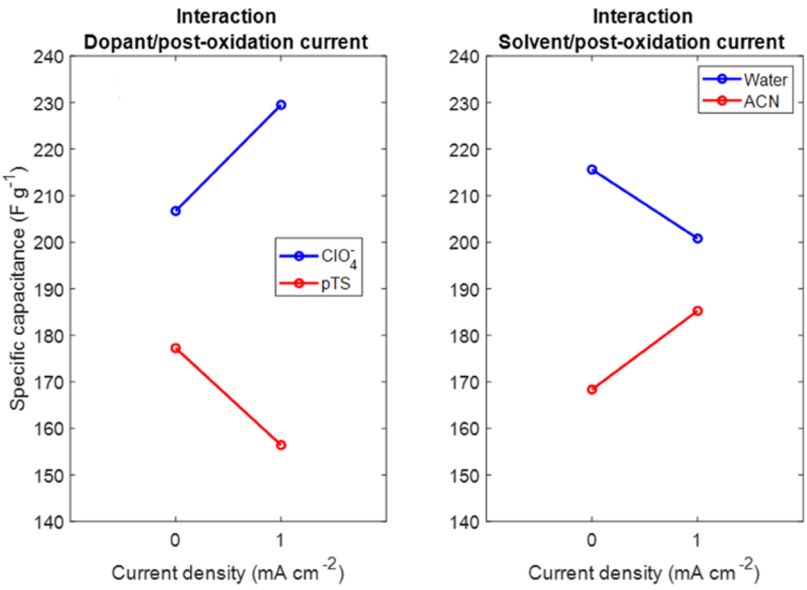

Figure 13. Interaction plots for PPy coatings synthesized by method A.

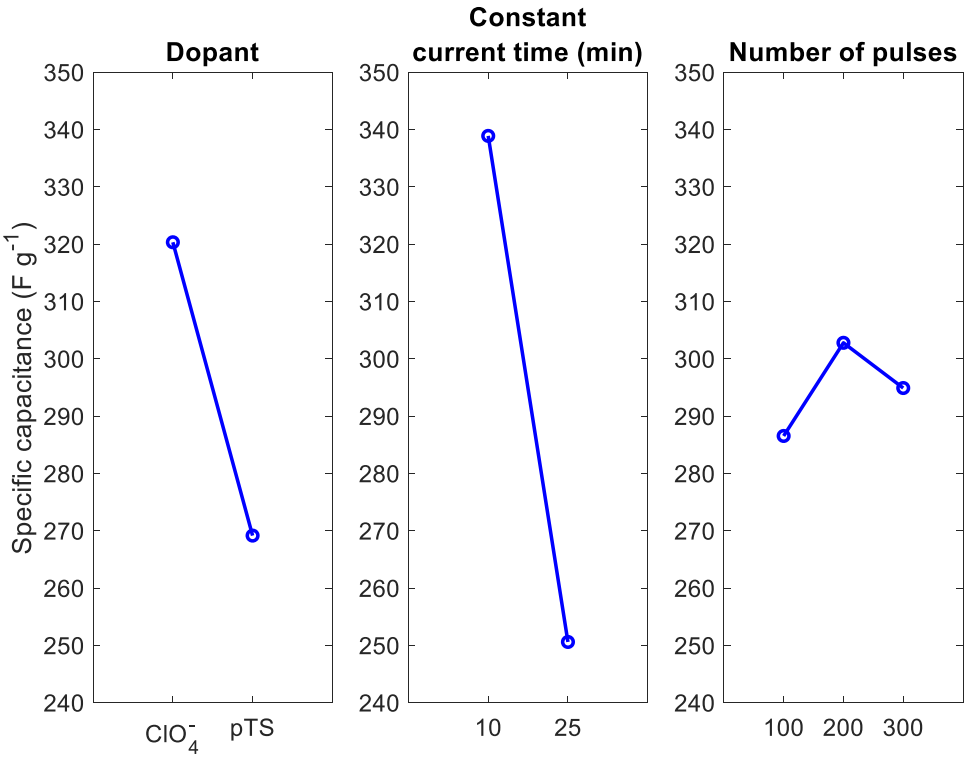

Figure 14. Main effects plot for PPy coatings synthesized by method B.

3.3. Design of Experiments and Statistical Analysis. Statistical analysis of the capacitance obtained by GCD was performed for all polymers. The ANOVA results for synthesis method A (Table S1) indicate that the post-oxidation, dopant/solvent interaction, and dopant/solvent/post-oxidation interactions are not statistically significant for the capacitive response of PPy and can be removed from the model. However, by the hierarchy principle, post-oxidation should not be overruled because its interactions have statistically significant effect.[59] The plot of the main effects for synthetic method A (Figure 12) indicates that there is a huge decrease in capacitance when going from ClO_4^- to pTS and from water to ACN. As mentioned in the Raman analysis of the polymer, the signals of the ClO_4^--doped PPy denote a higher level of doping, which can be associated with a better capacitive response. In the case of ACN, it is well known that this solvent generates more compact polymer coatings,[30] which hinders the diffusion of ions into the matrix in comparison with the polymer synthesized in water. This results in a lower participation of the active material in the charging/discharging process.

Because of the presence of interactions, the main effects plot must be interpreted carefully, also considering second-order effects. The increase in specific capacitance when a post-

https://doi.org/10.1021/acsomega.1c06843
ACS Omega 2022, 7, 15580−15595

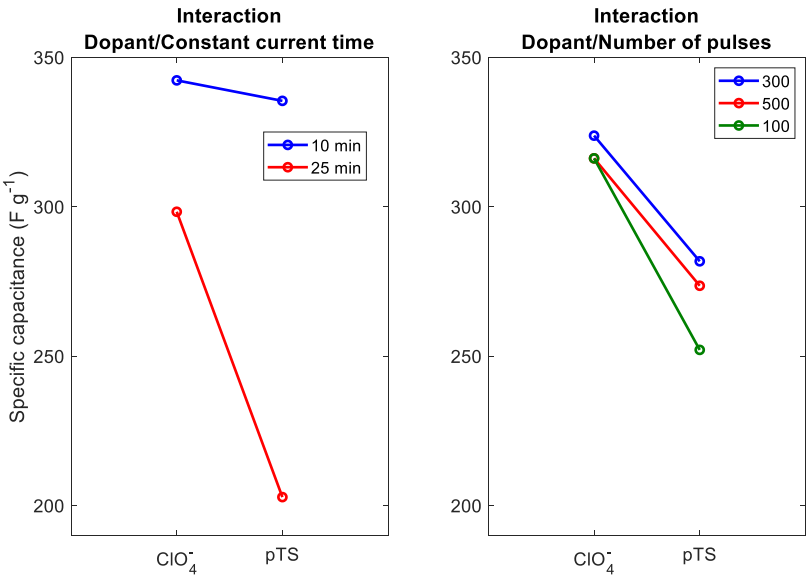

Figure 15. Interaction plot for PPy coatings synthesized by synthetic method B.

oxidation current is applied to ClO_4^--doped PPy, and the opposite effect when the dopant is pTS (Figure 13), is probably related to the size of the anion. When the polymer is exposed to an oxidation current, positive charges are formed on its chains. These charges are balanced by anions diffusing from solution. Because pTS is a large anion and polymers doped with this ion tend to form compact structures,[19,20] its insertion into the polymeric matrix is slower than with smaller ions such as ClO_4^-. Consequently, the nonstabilized cations can react with the polymer or with water molecules, causing overoxidation and degradation of the material, decreasing its capacitance. In the case of ClO_4^-, its diffusion in the polymer matrix is faster due to its small size, stabilizing the positive charges, preventing the overoxidation of the polymer, and increasing the doping level and, ultimately, the capacitance during the post-oxidation process. In the case of the solvent/post-oxidation current interaction (Figure 13), when the polymer is synthesized in water, the application of the post-oxidation current causes the decrease of its capacitance, and the opposite effect is observed when it is synthesized in ACN. This may be related to the difference in reactivity of the solvents. It is well known that during synthesis, the nonstabilized cations of PPy react with water, causing overoxidation of the material.[60] In contrast, the lower reactivity of ACN gives more time for the anions in solution to diffuse into the polymeric matrix and stabilize the positive charges by doping.

For synthesis method B, the ANOVA results (Table S2) indicate that all factors have a statistically significant influence on the PPy capacitance, except for the interaction "constant current application time/number of pulses". However, by the hierarchy principle, this term cannot be eliminated from the model because the interaction of all of the parameters is significant. From the main effects plot (Figure 14), the most important parameters are dopant and constant current time. The effect of the dopant was mentioned previously. For the constant current, the highest capacitance was observed when it was applied to the polymer for 10 min. This may be attributed to less pore coalescence due to the continuous growth of the polymer.[19,61]

The interaction plot for constant current time/dopant indicates a strong influence on the capacitive response due to the nonparallel behavior of the lines (Figure 15). For 10 min, the slight reduction in capacitance when using pTS as dopant is mainly ascribed to the compact structure of the polymer. Since a low current density (0.6 mA cm^{-2}) was used, the amount of polymer formed by this current was small and there is no significant reduction in ion mobility.

For 25 min, the reduction in supercapacitance is attributed to pore coalescence in combination with the compact structure of PPy-pTS. As more polymer is formed by the application of the constant current, the porosity decreases due to coalescence,[19,61] hampering the diffusion of ions into the inner part of the polymer. Thus, the amount of active material that participates in the charge/discharge process is significantly decreased. In the case of the number of pulses/dopant interaction, the almost parallel behavior of the lines indicates that there is no strong interaction between these parameters.

4. CONCLUSIONS

This study demonstrated the importance of considering the interactions between the synthesis parameters when obtaining conductive polymers for charge storage. The results showed that method B produces polymers of higher capacitance than method A, attributable to better ionic diffusion at the electrode/electrolyte interface and through the polymer matrix. ANOVA showed that with this method, all of the main factors have a significant effect on the capacitance of PPy, the highest capacitance (353.7 F g^{-1}) was obtained with PPy/ClO_4 synthesized with 300 pulses and application of 0.6 mA cm^{-2} at the end for 10 min. Acetonitrile showed disadvantages, compared to water, by favoring the formation of more compact polymers that hinder ionic mobility. PPy/pTS showed high cycling stability; however, due to the compact nature of this polymer, it would be necessary to use it at a very low thickness for good results in energy storage.

https://doi.org/10.1021/acsomega.1c06843
ACS Omega 2022, 7, 15580−15595

■ ASSOCIATED CONTENT

Supporting Information

The Supporting Information is available free of charge at https://pubs.acs.org/doi/10.1021/acsomega.1c06843.

Particle size distribution in PPy coatings from SEM; supporting SEM images; Nyquist plot of polymers taken from 1 mHz to 10 Hz; and verification of assumptions for ANOVA calculations and ANOVA test for the capacitance of polymers synthesized by methods A and B, measured at 1 A g^{-1} (PDF)

■ AUTHOR INFORMATION

Corresponding Author

María T. Cortés − *Department of Chemistry, Universidad de los Andes, Bogotá 111711, Colombia;* orcid.org/0000-0002-7475-2083; Email: marcorte@uniandes.edu.co

Authors

Andrés F. Pérez-Torres − *Department of Chemistry, Universidad de los Andes, Bogotá 111711, Colombia*

Martín González-Hernández − *Department of Chemistry, Universidad de los Andes, Bogotá 111711, Colombia*

Pablo Ortiz − *Department of Chemical Engineering, Universidad de los Andes, Bogotá 111711, Colombia*

Complete contact information is available at: https://pubs.acs.org/10.1021/acsomega.1c06843

Author Contributions

A.F.P.-T., M.T.C., M.G.-H., and P.O. contributed to conceptualization. A.F.P.-T. involved in experimentation; A.F.P.-T. performed writing—original draft preparation. A.F.P.-T., M.T.C., and P.O. performed writing—review and editing. All authors have read and agreed to the published version of the manuscript.

Notes

The authors declare no competing financial interest.

■ ACKNOWLEDGMENTS

A.F.P-T, M.E.G and M.T.C. thank the Department of Chemistry, Faculty of Science (Project INV-2021-128-2285). P.O. thanks the Department of Chemical Engineering. The authors would like to thank the Vice Presidency of Research & Creation's Publication Fund at Universidad de los Andes for its financial support (INV-2022-135-2351).

■ ABBREVIATIONS

ACN, acetonitrile; DOE, design of experiments; PPy, polypyrrole; pTS, *p*-toluenesulfonate ion

■ REFERENCES

(1) Wang, J.; Dong, S.; Ding, B.; Wang, Y.; Hao, X.; Dou, H.; Xia, Y.; Zhang, X. Pseudocapacitive Materials for Electrochemical Capacitors: From Rational Synthesis to Capacitance Optimization. *Natl. Sci. Rev.* **2017**, *4*, 71−90.

(2) Bakker, M. G.; Frazier, R. M.; Burkett, S.; Bara, J. E.; Chopra, N.; Spear, S.; Pan, S.; Xu, C. Perspectives on Supercapacitors, Pseudocapacitors and Batteries. *Nanomater. Energy* **2012**, *1*, 136−158.

(3) Goodenough, J. B. Energy Storage Materials: A Perspective. *Energy Storage Mater.* **2015**, *1*, 158−161.

(4) Yang, J.; Liu, Y.; Liu, S.; Li, L.; Zhang, C.; Liu, T. Conducting Polymer Composites: Material Synthesis and Applications in Electrochemical Capacitive Energy Storage. *Mater. Chem. Front.* **2017**, *1*, 251−268.

(5) Wu, Z.; Li, L.; Yan, J.; Zhang, X. Materials Design and System Construction for Conventional and New-Concept Supercapacitors. *Adv. Sci.* **2017**, *4*, No. 1600382.

(6) Bryan, A. M.; Santino, L. M.; Lu, Y.; Acharya, S.; D'Arcy, J. M. Conducting Polymers for Pseudocapacitive Energy Storage. *Chem. Mater.* **2016**, *28*, 5989−5998.

(7) Aguirre, J. C.; Ferreira, A.; Ding, H.; Jenekhe, S. A.; Kopidakis, N.; Asta, M.; Pilon, L.; Rubin, Y.; Tolbert, S. H.; Schwartz, B. J.; Dunn, B.; Ozolins, V. Panoramic View of Electrochemical Pseudocapacitor and Organic Solar Cell Research in Molecularly Engineered Energy Materials (MEEM). *J. Phys. Chem. C* **2014**, *118*, 19505−19523.

(8) Jiang, Y.; Liu, J. Definitions of Pseudocapacitive Materials: A Brief Review. *Energy Environ. Mater.* **2019**, *2*, 30−37.

(9) Dubal, D. P.; Lee, S. H.; Kim, J. G.; Kim, W. B.; Lokhande, C. D. Porous Polypyrrole Clusters Prepared by Electropolymerization for a High Performance Supercapacitor. *J. Mater. Chem.* **2012**, *22*, 3044−3052.

(10) Dubal, D. P.; Patil, S. V.; Jagadale, A. D.; Lokhande, C. D. Two Step Novel Chemical Synthesis of Polypyrrole Nanoplates for Supercapacitor Application. *J. Alloys Compd.* **2011**, *509*, 8183−8188.

(11) Snook, G. A.; Kao, P.; Best, A. S. Conducting-Polymer-Based Supercapacitor Devices and Electrodes. *J. Power Sources* **2011**, *196*, 1−12.

(12) Choudhary, R. B.; Ansari, S.; Purty, B. Robust Electrochemical Performance of Polypyrrole (PPy) and Polyindole (PIn) Based Hybrid Electrode Materials for Supercapacitor Application: A Review. *J. Energy Storage* **2020**, *29*, No. 101302.

(13) Du, H.; Xie, Y.; Xia, C.; Wang, W.; Tian, F. Electrochemical Capacitance of Polypyrrole−Titanium Nitride and Polypyrrole−Titania Nanotube Hybrids. *New J. Chem.* **2014**, *38*, 1284−1293.

(14) Mohd Abdah, M. A. A.; Azman, N. H. N.; Kulandaivalu, S.; Sulaiman, Y. Review of the Use of Transition-Metal-Oxide and Conducting Polymer-Based Fibres for High-Performance Supercapacitors. *Mater. Des.* **2020**, *186*, No. 108199.

(15) Wannapob, R.; Vagin, M. Yu.; Jeerapan, I.; Mak, W. C. Pure Nanoscale Morphology Effect Enhancing the Energy Storage Characteristics of Processable Hierarchical Polypyrrole. *Langmuir* **2015**, *31*, 11904−11913.

(16) Arcila-Velez, M. R.; Roberts, M. E. Redox Solute Doped Polypyrrole for High-Charge Capacity Polymer Electrodes. *Chem. Mater.* **2014**, *26*, 1601−1607.

(17) Huang, Y.; Zhi, C. Functional Flexible and Wearable Supercapacitors. *J. Phys. Appl. Phys.* **2017**, *50*, No. 273001.

(18) Zhao, J.; Wu, J.; Li, B.; Du, W.; Huang, Q.; Zheng, M.; Xue, H.; Pang, H. Facile Synthesis of Polypyrrole Nanowires for High-Performance Supercapacitor Electrode Materials. *Prog. Nat. Sci. Mater. Int.* **2016**, *26*, 237−242.

(19) Wang, J.; Wu, C.; Wu, P.; Li, X.; Zhang, M.; Zhu, J. Polypyrrole Capacitance Characteristics with Different Doping Ions and Thicknesses. *Phys. Chem. Chem. Phys.* **2017**, *19*, 21165−21173.

(20) Raudsepp, T.; Marandi, M.; Tamm, T.; Sammelselg, V.; Tamm, J. Study of the Factors Determining the Mobility of Ions in the Polypyrrole Films Doped with Aromatic Sulfonate Anions. *Electrochim. Acta* **2008**, *53*, 3828−3835.

(21) Otero, T. F.; Cantero, I.; Grande, H. Solvent Effects on the Charge Storage Ability in Polypyrrole. *Electrochim. Acta* **1999**, *44*, 2053−2059.

(22) Sharma, R. K.; Rastogi, A. C.; Desu, S. B. Pulse Polymerized Polypyrrole Electrodes for High Energy Density Electrochemical Supercapacitor. *Electrochem. Commun.* **2008**, *10*, 268−272.

(23) Li, C. M.; Sun, C. Q.; Chen, W.; Pan, L. Electrochemical Thin Film Deposition of Polypyrrole on Different Substrates. *Surf. Coat. Technol.* **2005**, *198*, 474−477.

(24) Kumar, A.; Singh, R. K.; Agarwal, K.; Singh, H. K.; Srivastava, P.; Singh, R. Effect of P-Toluenesulfonate on Inhibition of Overoxidation of Polypyrrole. *J. Appl. Polym. Sci.* **2013**, *130*, 434−442.

(25) Wang, J.; Xu, Y.; Chen, X.; Du, X.; Li, X. Effect of Doping Ions on Electrochemical Capacitance Properties of Polypyrrole Films. *Acta Phys.-Chim. Sin.* **2007**, *23*, 299−304.
(26) Huang, Y.; Zhu, M.; Pei, Z.; Huang, Y.; Geng, H.; Zhi, C. Extremely Stable Polypyrrole Achieved via Molecular Ordering for Highly Flexible Supercapacitors. *ACS Appl. Mater. Interfaces* **2016**, *8*, 2435−2440.
(27) Wang, J.; Xu, Y.; Wang, J.; Du, X.; Xiao, F.; Li, J. High Charge/Discharge Rate Polypyrrole Films Prepared by Pulse Current Polymerization. *Synth. Met.* **2010**, *160*, 1826−1831.
(28) Du, X.; Hao, X.; Wang, Z.; Ma, X.; Guan, G.; Abuliti, A.; Ma, G.; Liu, S. Highly Stable Polypyrrole Film Prepared by Unipolar Pulse Electro-Polymerization Method as Electrode for Electrochemical Supercapacitor. *Synth. Met.* **2013**, *175*, 138−145.
(29) Zhang, J.; Kong, L.-B.; Li, H.; Luo, Y.-C.; Kang, L. Synthesis of Polypyrrole Film by Pulse Galvanostatic Method and Its Application as Supercapacitor Electrode Materials. *J. Mater. Sci.* **2010**, *45*, 1947−1954.
(30) Vernitskaya, T. V.; Efimov, O. N. Polypyrrole: A Conducting Polymer; Its Synthesis, Properties and Applications. *Russ. Chem. Rev.* **1997**, *66*, 443.
(31) Tamm, J.; Raudsepp, T.; Marandi, M.; Tamm, T. Electrochemical Properties of the Polypyrrole Films Doped with Benzenesulfonate. *Synth. Met.* **2007**, *157*, 66−73.
(32) Zhu, M.; Meng, W.; Huang, Y.; Huang, Y.; Zhi, C. Proton-Insertion-Enhanced Pseudocapacitance Based on the Assembly Structure of Tungsten Oxide. *ACS Appl. Mater. Interfaces* **2014**, *6*, 18901−18910.
(33) Ge, Y.; Xie, X.; Roscher, J.; Holze, R.; Qu, Q. How to Measure and Report the Capacity of Electrochemical Double Layers, Supercapacitors, and Their Electrode Materials. *J. Solid State Electrochem.* **2020**, *24*, 3215−3230.
(34) Hallik, A.; Alumaa, A.; Kurig, H.; Jänes, A.; Lust, E.; Tamm, J. On the Porosity of Polypyrrole Films. *Synth. Met.* **2007**, *157*, 1085−1090.
(35) Chen, S.; Cheng, H.; Tian, D.; Li, Q.; Zhong, M.; Chen, J.; Hu, C.; Ji, H. Controllable Synthesis, Core-Shell Nanostructures, and Supercapacitor Performance of Highly Uniform Polypyrrole/Polyaniline Nanospheres. *ACS Appl. Energy Mater.* **2021**, *4*, 3701−3711.
(36) Ma, S.; Li, W.; Cao, J.; Wang, X.; Xie, Y.; Deng, L.; Liu, H.; Huang, Z.; Sun, L.; Cheng, S. Flexible Planar Microsupercapacitors Based on Polypyrrole Nanotubes. *ACS Appl. Energy Mater.* **2021**, *4*, 8857−8865.
(37) Yue, T.; Hou, R.; Liu, X.; Qi, K.; Chen, Z.; Qiu, Y.; Guo, X.; Xia, B. Y. Hybrid Architecture of a Porous Polypyrrole Scaffold Loaded with Metal−Organic Frameworks for Flexible Solid-State Supercapacitors. *ACS Appl. Energy Mater.* **2020**, *3*, 11920−11928.
(38) Zhang, Y.; Shang, Z.; Shen, M.; Chowdhury, S. P.; Ignaszak, A.; Sun, S.; Ni, Y. Cellulose Nanofibers/Reduced Graphene Oxide/Polypyrrole Aerogel Electrodes for High-Capacitance Flexible All-Solid-State Supercapacitors. *ACS Sustainable Chem. Eng.* **2019**, *7*, 11175−11185.
(39) Bisquert, J.; Belmonte, G. G.; Santiago, F. F.; Ferriols, N. S.; Yamashita, M.; Pereira, E. C. Application of a Distributed Impedance Model in the Analysis of Conducting Polymer Films. *Electrochem. Commun.* **2000**, *2*, 601−605.
(40) Garcia-Belmonte, G.; Bisquert, J. Impedance Analysis of Galvanostatically Synthesized Polypyrrole Films. Correlation of Ionic Diffusion and Capacitance Parameters with the Electrode Morphology. *Electrochim. Acta* **2002**, *47*, 4263−4272.
(41) Marchesi, L. F. Q. P.; Simões, F. R.; Pocrifka, L. A.; Pereira, E. C. Investigation of Polypyrrole Degradation Using Electrochemical Impedance Spectroscopy. *J. Phys. Chem. B* **2011**, *115*, 9570−9575.
(42) Bhalerao, A. B.; Bulakhe, R. N.; Deshmukh, P. R.; Shim, J.-J.; Nandurkar, K. N.; Wagh, B. G.; Vattikuti, S. V. P.; Lokhande, C. D. Chemically Synthesized 3D Nanostructured Polypyrrole Electrode for High Performance Supercapacitor Applications. *J. Mater. Sci. Mater. Electron.* **2018**, *29*, 15699−15707.
(43) Wang, P.; Zheng, Y.; Li, B. Preparation and Electrochemical Properties of Polypyrrole/Graphite Oxide Composites with Various Feed Ratios of Pyrrole to Graphite Oxide. *Synth. Met.* **2013**, *166*, 33−39.
(44) Zhou, Y.; Wang, P.; Hu, M.; Tian, X. Charge Carrier Related Superior Capacitance of the Precisely Size-Controlled Polypyrrole Nanoparticles. *Electrochim. Acta* **2017**, *249*, 290−300.
(45) Wolfart, F.; Dubal, D. P.; Vidotti, M.; Holze, R.; Gómez-Romero, P. Electrochemical Supercapacitive Properties of Polypyrrole Thin Films: Influence of the Electropolymerization Methods. *J. Solid State Electrochem.* **2016**, *20*, 901−910.
(46) Ramya, R.; Sangaranarayanan, M. V. Analysis of Polypyrrole-Coated Stainless Steel Electrodes — Estimation of Specific Capacitances and Construction of Equivalent Circuits. *J. Chem. Sci.* **2008**, *120*, 25−31.
(47) Vadivel Murugan, A.; Reddy, M. V.; Campet, G.; Vijayamohanan, K. Cyclic Voltammetry, Electrochemical Impedance and Ex Situ X-Ray Diffraction Studies of Electrochemical Insertion and Deinsertion of Lithium Ion into Nanostructured Organic−Inorganic Poly(3,4-Ethylenedioxythiophene) Based Hybrids. *J. Electroanal. Chem.* **2007**, *603*, 287−296.
(48) Ko, J. S.; Sassin, M. B.; Rolison, D. R.; Long, J. W. Deconvolving Double-Layer, Pseudocapacitance, and Battery-like Charge-Storage Mechanisms in Nanoscale LiMn2O4 at 3D Carbon Architectures. *Electrochim. Acta* **2018**, *275*, 225−235.
(49) Ko, J. S.; Lai, C.-H.; Long, J. W.; Rolison, D. R.; Dunn, B.; Nelson Weker, J. Differentiating Double-Layer, Psuedocapacitance, and Battery-like Mechanisms by Analyzing Impedance Measurements in Three Dimensions. *ACS Appl. Mater. Interfaces* **2020**, *12*, 14071−14078.
(50) Jenden, C. M.; Davidson, R. G.; Turner, T. G. A Fourier Transform-Raman Spectroscopic Study of Electrically Conducting Polypyrrole Films. *Polymer* **1993**, *34*, 1649−1652.
(51) Viau, L.; Hihn, J. Y.; Lakard, S.; Moutarlier, V.; Flaud, V.; Lakard, B. Full Characterization of Polypyrrole Thin Films Electrosynthesized in Room Temperature Ionic Liquids, Water or Acetonitrile. *Electrochim. Acta* **2014**, *137*, 298−310.
(52) Wei, H.; Wang, Y.; Guo, J.; Yan, X.; O'Connor, R.; Zhang, X.; Shen, N. Z.; Weeks, B. L.; Huang, X.; Wei, S.; Guo, Z. Electropolymerized Polypyrrole Nanocoatings on Carbon Paper for Electrochemical Energy Storage. *ChemElectroChem* **2015**, *2*, 119−126.
(53) Hou, Y.; Zhang, L.; Chen, L. Y.; Liu, P.; Hirata, A.; Chen, M. W. Raman Characterization of Pseudocapacitive Behavior of Polypyrrole on Nanoporous Gold. *Phys. Chem. Chem. Phys.* **2014**, *16*, 3523−3528.
(54) Politi, S.; Carcione, R.; Tamburri, E.; Matassa, R.; Lavecchia, T.; Angjellari, M.; Terranova, M. L. Graphene Platelets from Shungite Rock Modulate Electropolymerization and Charge Storage Mechanisms of Soft-Template Synthetized Polypyrrole-Based Nanocomposites. *Sci. Rep.* **2018**, *8*, No. 17045.
(55) Trchová, M.; Stejskal, J. Resonance Raman Spectroscopy of Conducting Polypyrrole Nanotubes: Disordered Surface versus Ordered Body. *J. Phys. Chem. A* **2018**, *122*, 9298−9306.
(56) Santos, M. J. L.; Brolo, A. G.; Girotto, E. M. Study of Polaron and Bipolaron States in Polypyrrole by in Situ Raman Spectroelectrochemistry. *Electrochim. Acta* **2007**, *52*, 6141−6145.
(57) Zerbi, G.; Veronelli, M.; Martina, S.; Schlüter, A. D.; Wegner, G. Delocalization Length and Structure of Oligopyrroles and of Polypyrrole from Their Vibrational Spectra. *J. Chem. Phys.* **1994**, *100*, 978−984.
(58) Bhargava, P.; Liu, W.; Pope, M.; Tsui, T.; Yu, A. Substrate Comparison for Polypyrrole-Graphene Based High-Performance Flexible Supercapacitors. *Electrochim. Acta* **2020**, *358*, No. 136846.
(59) Montgomery, D. C. Introduction to Factorial Designs. In *Design and Analysis of Experiments*; John Wiley & Sons: New Jersey, 2013; pp 183−225.
(60) Debiemme-Chouvy, C.; Tran, T. T. M. An Insight into the Overoxidation of Polypyrrole Materials. *Electrochem. Commun.* **2008**, *10*, 947−950.

https://doi.org/10.1021/acsomega.1c06843
ACS Omega 2022, 7, 15580−15595

(61) Debiemme-Chouvy, C.; Fakhry, A.; Pillier, F. Electrosynthesis of Polypyrrole Nano/Micro Structures Using an Electrogenerated Oriented Polypyrrole Nanowire Array as Framework. *Electrochim. Acta* **2018**, *268*, 66−72.

https://doi.org/10.1021/acsomega.1c06843
ACS Omega 2022, 7, 15580−15595